A Comprehensive Cell Capacitor Energy Control Strategy of a Modular Multilevel Converter (MMC) without a Stiff DC Bus Voltage Source

Shenghui Cui, Sungmin Kim, Jae-Jung Jung, and Seung-Ki Sul
Department of Electrical and Computer Engineering
Seoul National University
Seoul, Korea
choish@eepel.snu.ac.kr, ksmin@eepel.snu.ac.kr, jaejung.jung@eepel.snu.ac.kr, sulsk@plaza.snu.ac.kr

***Abstract*— Cell capacitor energy control of a Modular Multilevel Converter (MMC) is conventionally done by controlling leg current and modulation strategy. In most of literatures, leg current transient is analyzed under an assumption that the DC bus is a stiff DC voltage source. In a real MMC-based HVDC transmission system, however, there's no such virtual stiff DC voltage source and the conventional regulation method can lead to poor dynamics of cell capacitor energy control and even make system unstable. In this paper, the MMC model is revised for circulating current transient analysis. Based on the revised model, a new comprehensive cell capacitor energy control strategy is proposed by updating leg capacitor energy reference on-line and injecting positive and negative sequence circulating currents. Validity of the proposed method is verified by a 7-level scaled version prototype experimental setup.**

I. INTRODUCTION

Voltage Source Converter (VSC) based High Voltage Direct Current (HVDC) transmission is a promising solution for future smart grid which would integrate a great amount of renewable energy sources. For VSC-HVDC, compared to the conventional two level or three level converters, a Modular Multilevel Converter (MMC) is a competitive candidate and attracting worldwide attention [1-3]. MMC presents many advantages such as very low harmonics, low dv/dt, modularity and simple scaling, no necessity of series connection of power semiconductors, and DC bus capacitor elimination [4-6], etc.

For each AC-DC converter in VSC-HVDC, there should be several controllers such as an active power controller implemented in the form of a fixed active power controller, a fixed DC bus voltage controller, or a frequency controller and a reactive power controller implemented in the form of a fixed reactive power controller or a fixed Point of Common Coupling (PCC) voltage controller. For a point-to-point VSC-HVDC transmission system, one station should operate in fixed DC bus voltage control mode (namely rectifier mode) to regulate transmission line voltage[7].

Cell capacitor energy control is one of the main concerns in MMC. Conventionally, cell capacitor energy control has been realized by controlling leg current [8-9] and modulation strategy. The leg capacitor energy was controlled by regulating the DC component of the leg current, and the upper and lower arm capacitor energy in each leg was balanced by regulating line frequency component of the leg current [10,11]. Cell capacitor energy balancing in each arm is realized through modulation strategy such as Nearest Level Modulation (NLM) [12-13]. In most literatures, it's assumed that a stiff DC voltage source is connected to the DC bus of the MMC and the leg current regulation strategy was designed under such assumption. However, for the MMC operates at fixed DC bus voltage control mode, the DC bus is not stiff [14,15] and the conventional energy control strategy can lead to poor dynamics of cell capacitor energy balancing and even make the system unstable. In this paper, a MMC without the assumption of the stiff DC bus voltage source is proposed and modeled to analyze circulating current transient. Based on the proposed MMC model, a new comprehensive cell capacitor energy control strategy is proposed by updating leg capacitor energy reference on-line and injecting positive and negative sequence circulating currents.

In Section II, the conventional modeling and control

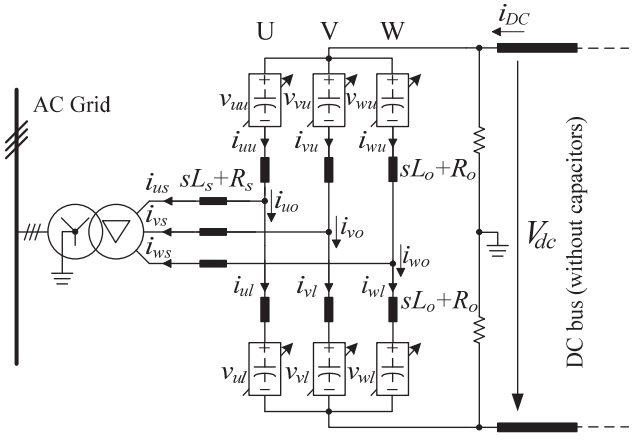

Figure 1. Simplified schematic of a MMC station in HVDC.

strategy is reviewed. In Section III, a new MMC model for HVDC application is proposed and analyzed. In the new model, MMC is divided into three extracted models: AC grid current model, DC bus current model, and circulating current model, respectively. In Section IV, principle and implementation method of the proposed cell capacitor energy control strategy are presented. In Section V, validity of the proposed control strategy is verified experimentally by a scaled experimental setup.

II. Conventional Modeling and Cell Capacitor Energy Control Strategy of MMC

A simplified schematic of a MMC station in HVDC is shown in Fig. 1. A MMC consists of three legs for three phases, and each leg consists of two arms. Each arm usually contains numerous (up to several hundreds) half bridge choppers and can be modeled as a high bandwidth controlled voltage source with a capacitor tank. The AC side of the MMC is connected to AC grid through a wye-delta transformer to avoid zero sequence current flowing into the MMC. The MMC is grounded by two equal high impedance voltage dividers between positive and negative poles of the DC bus.

In this paper, the average value of upper and lower arm currents of phase x is defined as leg current and denoted as i_{xo} as shown in (1).

$$i_{xo} = (i_{xu} + i_{xl})/2. \tag{1}$$

In the conventional modeling, the DC bus of the MMC is modeled as a voltage source and transient of leg current is analyzed independently for each phase. Per phase equivalent circuit of the conventional modeling is shown in Fig. 2 [10]. According to Kirchhoff's law, (2) and (3) can be deduced.

$$-\frac{v_{xu}-v_{xl}}{2} - v_{xg} = \{(\frac{R_o}{2}+R_s)+(\frac{L_o}{2}+L_s)\frac{d}{dt}\}i_{xs}. \tag{2}$$

$$V_{dc} - (v_{xu}+v_{xl}) = 2(R_o + L_o\frac{d}{dt})i_{xo}. \tag{3}$$

Output voltage and leg internal voltage are defined as (4) and (5) respectively.

$$v_{xs} = -\frac{v_{xu}-v_{xl}}{2}. \tag{4}$$

$$v_{xo} = \frac{V_{dc}-(v_{xu}+v_{xl})}{2}. \tag{5}$$

Substituting (4) and (5) into (2) and (3), output current and leg current can be deduced as follows:

$$v_{xs} - v_{xg} = \{(\frac{R_o}{2}+R_s)+(\frac{L_o}{2}+L_s)\frac{d}{dt}\}i_{xs}. \tag{6}$$

$$v_{xo} = (R_o + L_o\frac{d}{dt})i_{xo}. \tag{7}$$

From (6) and (7), it can be concluded that output voltage v_{xs} and leg internal voltage v_{xo} can be used to regulate output current and leg current independently. To generate desired v_{xs} and v_{xo}, upper and lower arm output voltages should be synthesized as (8) and (9).

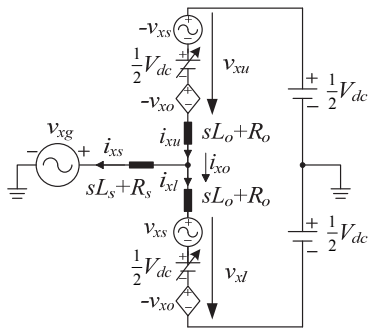

Figure 2. Per phase equivalent circuit of the conventional modeling.

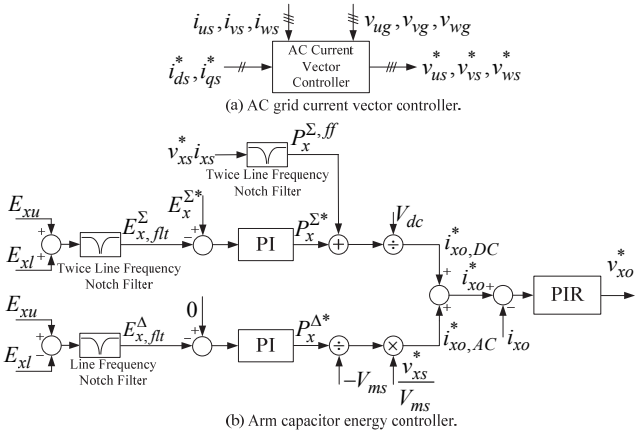

Figure 3. Conventional cascade structured arm capacitor energy controller.

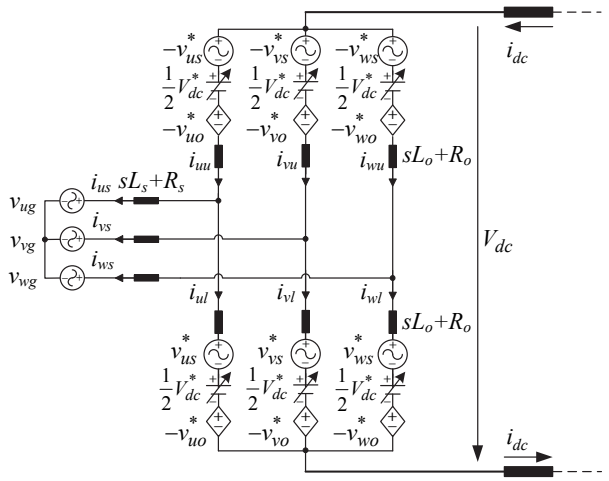

Figure 4. MMC model for HVDC application if the conventional control strategy is employed.

$$v^*_{xu} = \frac{V^*_{dc}}{2} - v^*_{xs} - v^*_{xo}. \tag{8}$$

$$v^*_{xl} = \frac{V^*_{dc}}{2} + v^*_{xs} - v^*_{xo}. \tag{9}$$

In (8) and (9), as a feed-forward variable, V^*_{dc} should be synthesized as (10).

$$V^*_{dc} = V_{dc}. \tag{10}$$

To control the arm capacitor energy, the power flow into each arm in a leg should be considered. Power that flows into upper and lower arms in the same phase *x* can be deduced as (11) and (12) respectively.

$$P_{xu} = \frac{dE_{xu}}{dt} = v_{xu}^* i_{xu} = (\frac{V_{dc}^*}{2} - v_{xs}^* - v_{xo}^*)(i_{xo} + \frac{1}{2} i_{xs}). \quad (11)$$

$$P_{xl} = \frac{dE_{xl}}{dt} = v_{xl}^* i_{xl} = (\frac{V_{dc}^*}{2} + v_{xs}^* - v_{xo}^*)(i_{xo} - \frac{1}{2} i_{xs}). \quad (12)$$

Then sum and difference of power that flows into upper and lower arms in the same leg of phase *x* are described as (13) and (14) respectively.

$$P_x^{\Sigma} = P_{xu} + P_{xl} = \frac{dE_x^{\Sigma}}{dt} = \frac{d(E_{xu} + E_{xl})}{dt} = V_{dc}^* i_{xo} - v_{xs}^* i_{xs} - 2 v_{xo}^* i_{xo}. \quad (13)$$

$$P_x^{\Delta} = P_{xu} - P_{xl} = \frac{dE_x^{\Delta}}{dt} = \frac{d(E_{xu} - E_{xl})}{dt} = \frac{1}{2} V_{dc}^* i_{xs} - 2 v_{xs}^* i_{xo} - v_{xo}^* i_{xs}. \quad (14)$$

For VSC-HVDC application, the third terms in the right sides of both (13) and (14) can be neglected [10]. In the conventional arm capacitor energy control strategy, the sum of upper and lower arm capacitor energy E_x^{Σ} was controlled by regulating the first term in the right side of (13), and the difference of upper and lower arm capacitor energy E_x^{Δ} was controlled by regulating the second term in the right side of (14). Thus, a DC component of leg current i_{xo} was injected to regulate E_x^{Σ}, and a line frequency component of leg current i_{xo} was injected to regulate E_x^{Δ}. A cascade structured controller consisted of an outer capacitor energy controller and an inner leg current regulator had been proposed in [11], as shown in Fig. 3. In [11], a Proportional-Integral-Resonant (PIR) controller was employed for leg current regulation and the resonant regulator resonates at line frequency ω_o. It should be noticed that since a considerable twice line frequency component and a line frequency component existed in E_x^{Σ} and E_x^{Δ} respectively, notch filters were employed.

III. Modification of MMC Modeling in HVDC Transmission

The conventional modeling and control strategy of the MMC are based on a stiff voltage source in the DC bus. Since actual DC bus of HVDC transmission reveals rather current source characteristic due to the inductances of the smoothing reactor and transmission cable, the conventional modeling is not valid for HVDC application and the conventional cell capacitor energy control strategy can lead to poor dynamics of cell capacitor energy control and even make system unstable. In Fig. 4, the circuit model of MMC is shown if the conventional control strategy is employed for HVDC application where DC link looks like current source. For phases *x* and *y*, according to Kirchhoff's law, transients of upper and lower arm currents can be described as (15) and (16).

$$\begin{cases} (-v_{xs}^* + V_{dc}^*/2 - v_{xo}^*) + (L_o \frac{d}{dt} + R_o) i_{xu} + (L_s \frac{d}{dt} + R_s) i_{xs} + v_{xg} \\ -(-v_{ys}^* + V_{dc}^*/2 - v_{yo}^*) - (L_o \frac{d}{dt} + R_o) i_{yu} - (L_s \frac{d}{dt} + R_s) i_{ys} - v_{yg} = 0. \end{cases} \quad (15)$$

$$\begin{cases} (v_{xs}^* + V_{dc}^*/2 - v_{xo}^*) + (L_o \frac{d}{dt} + R_o) i_{xl} - (L_s \frac{d}{dt} + R_s) i_{xs} - v_{xg} \\ -(v_{ys}^* + V_{dc}^*/2 - v_{yo}^*) - (L_o \frac{d}{dt} + R_o) i_{yl} + (L_s \frac{d}{dt} + R_s) i_{ys} + v_{yg} = 0. \end{cases} \quad (16)$$

And then (15) and (16) can be deduced as (17) and (18).

$$\begin{cases} -v_{xs}^* + (L_o \frac{d}{dt} + R_o)(i_{xs}/2) + (L_s \frac{d}{dt} + R_s) i_{xs} + v_{xg} \\ -(-v_{ys}^*) - (L_o \frac{d}{dt} + R_o)(i_{ys}/2) - (L_s \frac{d}{dt} + R_s) i_{ys} - v_{yg} = 0. \end{cases} \quad (17)$$

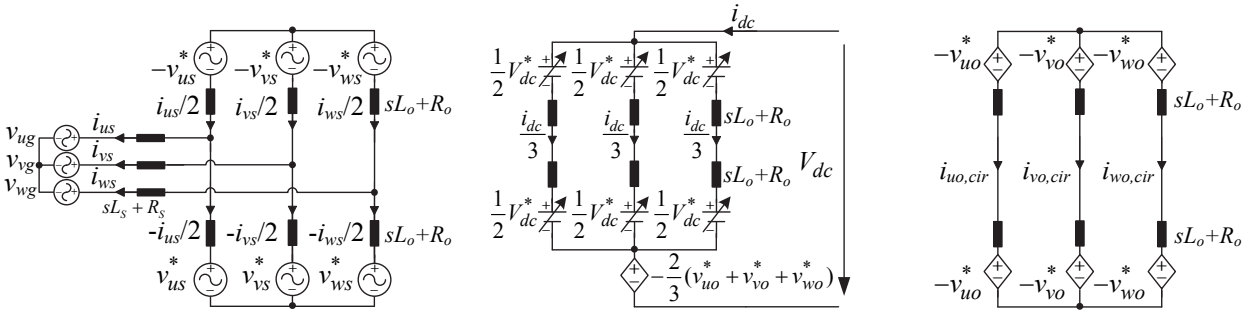

(a) Extracted model of AC grid current. (b) Extracted model of DC bus current. (c) Extracted model of circulating current.

Figure 5. Models extracted from the conventional MMC model to analyze AC grid current, DC bus current, and circulating current.

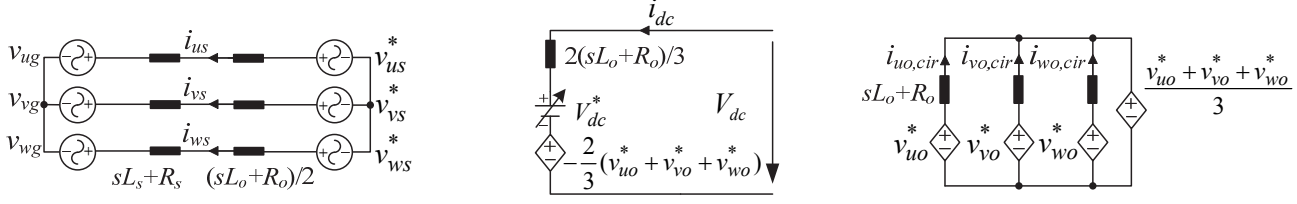

(a) Simplified equivalent model of AC grid current. (b) Simplified equivalent model of DC bus current. (c) Simplified equivalent model of circulating current.

Figure 6. Simplified equivalent models of AC grid current, DC bus current, and circulating current.

$$\begin{cases} v_{xs}^{*}+(L_o\frac{d}{dt}+R_o)(-i_{xs}/2)-(L_s\frac{d}{dt}+R_s)i_{xs}-v_{xg} \\ -(v_{ys}^{*})-(L_o\frac{d}{dt}+R_o)(-i_{ys}/2)+(L_s\frac{d}{dt}+R_s)i_{ys}+v_{yg}=0. \end{cases} \quad (18)$$

According to (17) and (18), a model to describe the AC grid current can be extracted from Fig. 4, as shown in Fig. 5(a). Subtracting (17) from (18), it can be deduced that:

$$\begin{cases} v_{xs}^{*}-\frac{1}{2}(L_o\frac{d}{dt}+R_o)i_{xs}-(L_s\frac{d}{dt}+R_s)i_{xs}-v_{xg} \\ -v_{ys}^{*}+\frac{1}{2}(L_o\frac{d}{dt}+R_o)i_{ys}+(L_s\frac{d}{dt}+R_s)i_{ys}+v_{yg}=0. \end{cases} \quad (19)$$

Then according to (19), the extracted model in Fig. 5(a) can be simplified as Fig. 6(a) equivalently. From (19) and Fig. 6(a), it can be concluded the AC grid current regulation of the conventional MMC control strategy is still valid for HVDC application.

In Fig. 4, the instantaneous value of the DC bus voltage V_{dc} can be calculated as (20), (21), and (22).

$$(-v_{us}^{*}+\frac{V_{dc}^{*}}{2}-v_{uo}^{*})+(L_o\frac{d}{dt}+R_o)(i_{uu}+i_{ul})+(v_{us}^{*}+\frac{V_{dc}^{*}}{2}-v_{uo}^{*})=V_{dc}. \quad (20)$$

$$(-v_{vs}^{*}+\frac{V_{dc}^{*}}{2}-v_{vo}^{*})+(L_o\frac{d}{dt}+R_o)(i_{vu}+i_{vl})+(v_{vs}^{*}+\frac{V_{dc}^{*}}{2}-v_{vo}^{*})=V_{dc}. \quad (21)$$

$$(-v_{ws}^{*}+\frac{V_{dc}^{*}}{2}-v_{wo}^{*})+(L_o\frac{d}{dt}+R_o)(i_{wu}+i_{wl})+(v_{ws}^{*}+\frac{V_{dc}^{*}}{2}-v_{wo}^{*})=V_{dc}. \quad (22)$$

Adding (20), (21), and (22), DC bus voltage can be described as (23).

$$V_{dc}=V_{dc}^{*}+2(R_o+L_o\frac{d}{dt})(\frac{i_{dc}}{3})-\frac{2}{3}(v_{uo}^{*}+v_{vo}^{*}+v_{wo}^{*}). \quad (23)$$

In accordance with Kirchhoff's current law and (23), a model for DC bus current can be extracted from Fig. 4, as shown in Fig. 5(b). The DC bus current model in Fig. 5(b) can be further simplified as shown in Fig. 6(b). Since the DC bus voltage is described as (23), the leg current of phase *x*, namely i_{xo} can be deduced as (24).

$$2(L_o\frac{d}{dt}+R_o)(i_{xo}-\frac{i_{dc}}{3})=2(v_{xo}^{*}-\frac{v_{uo}^{*}+v_{vo}^{*}+v_{wo}^{*}}{3}). \quad (24)$$

In this paper, a circulating current in phase *x*, $i_{xo,cir}$, is defined as the difference between leg current i_{xo} and the averaged current of the DC bus current that equally flows into each phase, as (25).

$$i_{xo,cir}=i_{xo}-\frac{i_{dc}}{3}. \quad (25)$$

Substituting (25) into (24), the circulating current of phase *x* can be described as (26).

$$2(L_o\frac{d}{dt}+R_o)i_{xo,cir}=2(v_{xo}^{*}-\frac{v_{uo}^{*}+v_{vo}^{*}+v_{wo}^{*}}{3}). \quad (26)$$

In accordance with (26), a model for three phase circulating currents can be extracted from Fig. 4, as shown in Fig. 5(c). It can be further simplified as Fig. 6(c). In summary, for HVDC application the MMC model in Fig. 4 can be divided into three extracted models in Fig. 5, which independently describe AC grid current, DC bus current, and circulating current.

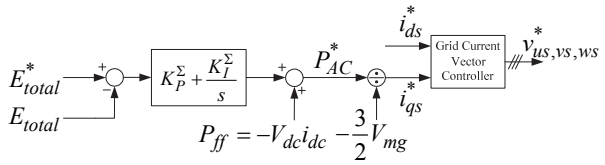

(a) Converter total capacitor energy control module for rectifier mode.

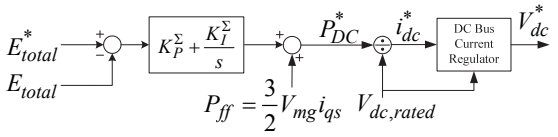

(b) Converter total capacitor energy control module for inverter mode.

Figure 7. Schematic of the proposed converter total capacitor energy controller.

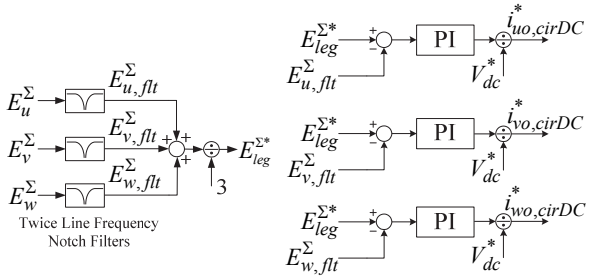

(a) Leg Energy Reference updating module. (b) Inter-leg energy balancing module.

Figure 8. Schematic of the proposed leg capacitor energy balancing controller.

In the conventional cell capacitor energy control strategy, the cell capacitor energy was controlled independently for each phase, which means that leg current of each phase was regulated independently. In this case a common mode voltage component defined as (27) can exist in three phase leg internal voltages if cell capacitor energy control and leg current regulation are implemented independently at each phase.

$$v_{o,com}^{*}=\frac{v_{uo}^{*}+v_{vo}^{*}+v_{wo}^{*}}{3}. \quad (27)$$

It's noticed in Fig. 6(b) that the common mode leg internal voltage $v_{o,com}^{*}$ would affect real DC bus voltage as (23). Moreover, it would also affect the circulating current as shown in Fig. 6(c) and it may accumulate a large DC component in $v_{o,com}^{*}$ as it is presented by experiment in Section V, and make the system unstable. Contrast to motor-drive application, the DC bus in the HVDC transmission system is not any more a stiff DC voltage source, and has rather current source characteristics, and the common mode leg internal voltage $v_{o,com}^{*}$ should be controlled as null. If a cell capacitor energy control strategy can nullify $v_{o,com}^{*}$ inherently, then AC current regulation, DC current regulation, and cell capacitor energy control can be completely decoupled and the MMC for HVDC may have better dynamic performance compared to conventional cell capacitor energy control strategy. Based on above observation, a new comprehensive cell capacitor control strategy is proposed in Section IV.

IV. PROPOSED CELL CAPACITOR ENERGY CONTROL STATEGY

Capacitor energy of the cells in the same arm can be easily balanced by corresponding modulation methods without affecting current regulation. The main target of cell capacitor energy control is controlling capacitor energy of six arms as rated value, E_{rated} , namely as (28), which is mathematically equivalent to (29)-(33).

$$E_{uu} = E_{ul} = E_{vu} = E_{vl} = E_{wu} = E_{wl} = E_{rated}. \quad (28)$$

$$E_{total} = \sum_{x=u,v,w} E_{xu} + E_{xl} = 6E_{rated}. \quad (29)$$

$$E_u^{\Sigma} = E_v^{\Sigma} = E_w^{\Sigma}. \quad (30)$$

$$E_u^{\Delta} = E_{uu} - E_{ul} = 0. \quad (31)$$

$$E_v^{\Delta} = E_{vu} - E_{vl} = 0. \quad (32)$$

$$E_w^{\Delta} = E_{wu} - E_{wl} = 0. \quad (33)$$

It should be noticed that the energy described as (29) means the energy stored in the whole MMC cell capacitors. Eq. (30) means inter-leg capacitor energy balancing, and (31)-(33) means upper and lower arm capacitor energy balancing for each phase.

A. Control of energy stored in the whole MMC cell capacitors

In the conventional leg capacitor energy control method, capacitor energy of each leg was controlled independently and energy exchanges between each leg and the stiff DC bus voltage source. If a MMC operates in rectifier mode to control DC bus voltage, the whole energy stored in the MMC should be regulated by controlling AC grid active power as shown in Fig. 7(a). In this paper it is assumed that the grid voltage vector is oriented to synchronously rotating q-axis. For a MMC operates in inverter mode, the converter total cell capacitor energy should be regulated by controlling DC bus power, namely by controlling DC bus current as shown in Fig. 7(b). As analyzed in Section III and shown in Fig. 6, regulating AC or DC current would not generate the common mode component of leg internal voltages.

B. Balancing of three phase leg capacitor energy

With weak DC link, meaning that DC link has rather current source characteristics without stiff DC voltage source, balancing of three phase leg energy and balancing of upper and lower arm energy should not affect AC grid and DC bus current regulation. In this case, the balancing should be implemented not by the common mode voltage which is usually employed for capacitor energy balancing in cascade full-bridge based STATCOMs, but by the power flowing inside the converter. The circulating current defined in Section III flows inside the converter and can transfer energy between arms without affecting AC grid current and DC bus current.

The proposed leg capacitor energy balancing schematic is shown in Fig. 8. Contrast to the conventional leg energy control method, the most important point of the proposed strategy is that the leg capacitor energy reference is updated every sampling period as the average capacitor energy of three legs, instead of a constant reference value. The philosophy of

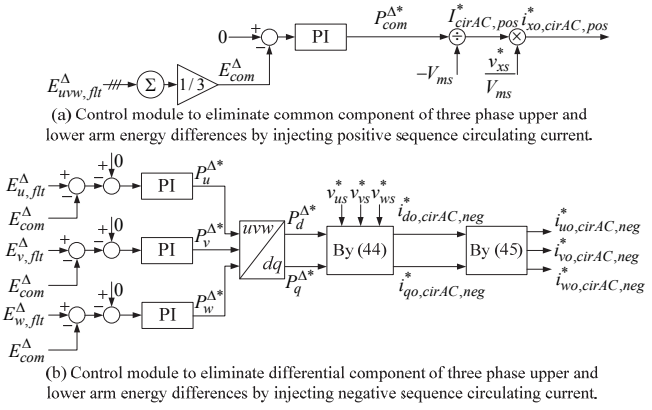

(a) Control module to eliminate common component of three phase upper and lower arm energy differences by injecting positive sequence circulating current.

(b) Control module to eliminate differential component of three phase upper and lower arm energy differences by injecting negative sequence circulating current.

Figure 9. Schematic of the proposed upper and lower arm capacitor energy balancing controller.

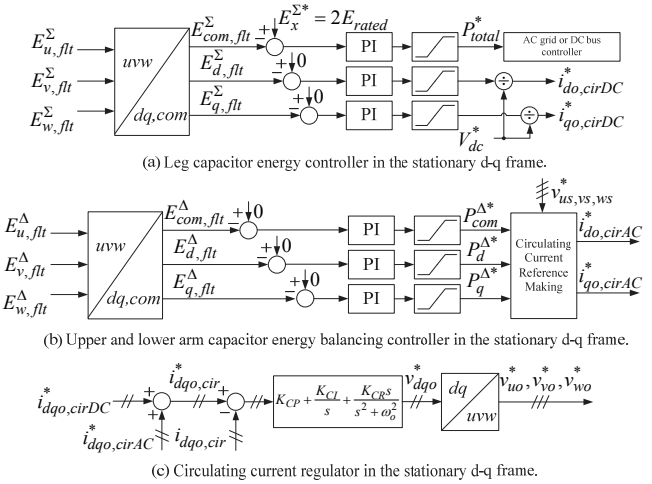

(a) Leg capacitor energy controller in the stationary d-q frame.

(b) Upper and lower arm capacitor energy balancing controller in the stationary d-q frame.

(c) Circulating current regulator in the stationary d-q frame.

Figure 10. Brief conceptual schematic of the proposed cascade structured cell capacitor energy controller in the stationary d-q frame.

the conventional leg capacitor energy control method was drawing power from the DC bus into each leg independently, while the philosophy of the proposed method is drawing power from AC grid or DC bus into the whole three phase converter and balancing inner-converter leg capacitor energy by circulating current. Since the leg capacitor energy reference is updated on-line as shown in Fig. 8(a), it can be deduced as (34).

$$\sum_{x=u,v,w} (E_{leg}^{\Sigma *} - E_{x,flt}^{\Sigma}) = 0. \Rightarrow \sum_{x=u,v,w} i_{xo,cirDC}^{*} = 0. \Rightarrow \sum_{x=u,v,w} v_{xo,DC}^{*} = 0. \quad (34)$$

Then in the proposed leg capacitor energy control method, the common mode component of leg internal voltages $v_{o,com}^{*}$ is inherently null. And, problems caused by $v_{o,com}^{*}$ such as poor dynamic and system stability issues can be inherently prevented. Since there is a considerable twice line frequency fluctuation in the leg capacitor energy, notch filters with a central frequency at twice line frequency are employed in the control loop in Fig.8 (a).

C. Balancing of upper and lower arm capacitor energy

With the proposed control strategy, the total capacitor energy in the MMC can be kept by the AC or DC side active

power, and the capacitor energy among three legs can be balanced by DC component of circulating currents. Next, the capacitor energy of upper and lower arms should be also balanced for each leg.

If the common voltage, $v^*_{o,com}$, set as null by the proposed energy balancing control strategy, the common mode component of references of the AC circulating current at line frequency should be zero as (35).

$$\sum_{x=u,v,w} v^*_{xo,AC} = 0 \;. \Rightarrow \sum_{x=u,v,w} i^*_{xo,cirAC} = 0. \tag{35}$$

Since the arm energy should be balanced at three legs, three Degree of Freedoms (DOFs) are necessary to regulate P^{Δ}_u , P^{Δ}_v , and P^{Δ}_w independently. In this paper, a positive sequence circulating current and a negative sequence circulating current are employed. If the three phase output voltages are defined as (36), then its corresponding space vector can be denoted by (37).

$$\begin{cases} v^*_{us} = V_{ms}\cos(\omega_o t + \varphi). \\ v^*_{vs} = V_{ms}\cos(\omega_o t + \varphi - 2\pi/3). \\ v^*_{ws} = V_{ms}\cos(\omega_o t + \varphi + 2\pi/3). \end{cases} \tag{36}$$

$$\mathbf{V_s} = V_{ms} e^{j(\omega_o t + \varphi)}. \tag{37}$$

If a positive sequence circulating current and a negative sequence circulating current is injected as (38) and (39), then according to (14), upper and lower arm active power difference of each phase caused by positive and negative sequence circulating currents can be calculated as (40) and (41).

$$\begin{cases} i^*_{uo,cirAC,pos} = I_{cirAC,pos}\cos(\omega_o t + \varphi_{pos}). \\ i^*_{vo,cirAC,pos} = I_{cirAC,pos}\cos(\omega_o t + \varphi_{pos} - 2\pi/3). \\ i^*_{wo,cirAC,pos} = I_{cirAC,pos}\cos(\omega_o t + \varphi_{pos} + 2\pi/3). \end{cases} \tag{38}$$

$$\begin{cases} i^*_{uo,cirAC,neg} = I_{cirAC,neg}\cos(\omega_o t + \varphi_{neg}). \\ i^*_{vo,cirAC,neg} = I_{cirAC,neg}\cos(\omega_o t + \varphi_{neg} + 2\pi/3). \\ i^*_{wo,cirAC,neg} = I_{cirAC,neg}\cos(\omega_o t + \varphi_{neg} - 2\pi/3). \end{cases} \tag{39}$$

$$\begin{cases} P^{\Delta}_{u,pos} = -V_{ms} I_{cirAC,pos}\cos(\varphi - \varphi_{pos}). \\ P^{\Delta}_{v,pos} = -V_{ms} I_{cirAC,pos}\cos(\varphi - \varphi_{pos}). \\ P^{\Delta}_{w,pos} = -V_{ms} I_{cirAC,pos}\cos(\varphi - \varphi_{pos}). \end{cases} \tag{40}$$

$$\begin{cases} P^{\Delta}_{u,neg} = -V_{ms} I_{cirAC,neg}\cos(\varphi_{neg} - \varphi). \\ P^{\Delta}_{v,neg} = -V_{ms} I_{cirAC,neg}\cos(\varphi_{neg} - \varphi - 2\pi/3). \\ P^{\Delta}_{w,neg} = -V_{ms} I_{cirAC,neg}\cos(\varphi_{neg} - \varphi + 2\pi/3). \end{cases} \tag{41}$$

In (40) and (41), if the positive sequence circulating current is in phase with the output voltage, namely $\varphi_{pos} = \varphi$,then $I_{cirAC,pos}, I_{cirAC,neg}, \varphi_{neg}$ provides three DOFs for arm energy balancing under the restriction of nullification of (27). From (40) and (41), the positive sequence circulating current can be injected to eliminate the common component, E^{Δ}_{com} , of three phase arm capacitor energy differences, and the negative sequence circulating current can be injected to eliminate the differential components, E^{Δ}_d and E^{Δ}_q of three phase upper and lower arm capacitor energy differences as (42).

$$\begin{cases} P^{\Delta}_{com} = \dfrac{dE^{\Delta}_{com}}{dt} = \dfrac{d}{dt}\{\dfrac{1}{3}(E^{\Delta}_u + E^{\Delta}_v + E^{\Delta}_w)\} = -V_{ms} I_{cirAC,pos}. \\ P^{\Delta}_d = \dfrac{dE^{\Delta}_d}{dt} = \dfrac{d}{dt}(\dfrac{2}{3}E^{\Delta}_u - \dfrac{1}{3}E^{\Delta}_v - \dfrac{1}{3}E^{\Delta}_w) = -V_{ms} I_{cirAC,neg}\cos(\varphi_{neg} - \varphi). \\ P^{\Delta}_q = \dfrac{dE^{\Delta}_q}{dt} = \dfrac{d}{dt}(\dfrac{\sqrt{3}}{3}E^{\Delta}_v - \dfrac{\sqrt{3}}{3}E^{\Delta}_w) = -V_{ms} I_{cirAC,neg}\sin(\varphi_{neg} - \varphi). \end{cases} \tag{42}$$

Since for lower and upper arm capacitor energy balancing, circulating current reference only includes positive and negative components, in accordance with (34), (43) can be concluded.

$$\sum_{x=u,v,w} i^*_{xo,cir} = \sum_{x=u,v,w} (i^*_{xo,cirDC} + i^*_{xo,cirAC}) = 0. \Rightarrow \sum_{x=u,v,w} v^*_{xo}. \tag{43}$$

The proposed arm capacitor energy balancing controller is presented in Fig. 9. The line frequency notch filters, which should be employed to eliminate fluctuating components, are omitted in the figure. To make reference value of negative sequence circulating current, (44) and (45) should be used.

$$i^*_{do,cirAC,neg} + j i^*_{qo,cirAC,neg} = \frac{P^{\Delta *}_d + j P^{\Delta *}_q}{-V_{ms}} e^{j(\omega_o t + \varphi)} = \frac{P^{\Delta *}_d + j P^{\Delta *}_q}{-V^2_{ms}} \mathbf{V_s}. \tag{44}$$

$$\begin{bmatrix} i^*_{uo,cirAC,neg} \\ i^*_{vo,cirAC,neg} \\ i^*_{wo,cirAC,neg} \end{bmatrix} = \begin{bmatrix} 1 & 0 \\ -\frac{1}{2} & -\frac{\sqrt{3}}{2} \\ -\frac{1}{2} & \frac{\sqrt{3}}{2} \end{bmatrix} \begin{bmatrix} i^*_{do,cirAC,neg} \\ i^*_{qo,cirAC,neg} \end{bmatrix}. \tag{45}$$

Practically, because of measurement error, EMI noise, limited precision of digital processing, and employment of output limiting blocks in controllers, nullification of $v^*_{o,com}$ may not be always guaranteed. To deal with this problem, the entire cell capacitor energy controller including a leg capacitor energy balancing controller, a upper and lower arm capacitor energy balancing controller, and a circulating current regulator can be totally constructed in stationary d-q reference frame as briefly shown in Fig. 10.

V. Experimental Verification of Proposed Method

As a laboratory test setup, a seven level MMC prototype has been constructed and it is tested with the proposed control strategy. Parameters of the prototype is given in Table. I. The DC bus of the MMC is connected to a R-L load directly and there's no any voltage source or capacitor in the DC bus, emulating practical long DC transmission cable.

Firstly, performance of the proposed control strategy is investigated without DC load. And, the R-L load is separated from the MMC DC bus by a circuit breaker. From Fig. 11, it can be noted that with the conventional leg energy control strategy, there's a large accumulating common mode component in the leg internal voltages. The common mode component is considerable to the DC bus voltage and distorts

the real DC bus voltage severely. While, with the proposed strategy, the common mode component of leg internal voltages is prevented inherently as shown in Fig. 12. Therefore, the distortion of the circulating current regulation caused by $v_{o,com}^{*}$ is prevented and the circulating current tracks its reference with excellent dynamics as shown in Fig. 13. In Fig. 14, at the first the MMC total capacitor energy controller in Fig. 7(a) is activated and the total capacitor energy is regulated to its rated reference value. Then the leg capacitor energy balancing controller is activated and three phase leg capacitor energy is balanced and converged to rated value (32.34 J). In Fig. 15, the upper and lower arm capacitor energy difference controllers in Fig. 9(a) and Fig. 9(b) are activated and the positive and negative sequence circulating currents are injected sequentially. It can be observed that the common component of upper and lower arm capacitor energy differences is eliminated by injecting the positive sequence circulating current, and the differential component of upper and lower arm capacitor energy differences is eliminated by injecting the negative sequence circulating current, respectively. From the figure it has been seen that the proposed control strategy at no load condition works as desired.

At the second, performance of the proposed control strategy is studied at loaded condition. The MMC is connected to the AC grid and all of the proposed controllers are activated before the converter is loaded. Then the circuit breaker between the MMC DC bus and the R-L load is switched on. It can be seen in Fig. 16 and Fig. 17 that after the converter is loaded, leg capacitor energy control, and upper and lower arm capacitor energy balancing is implemented well for each phase by the proposed comprehensive cell capacitor energy control strategy. In Fig. 18, the converter is drawing active current (q-axis current) from AC grid as soon as the converter is loaded and the converter can also operate like a STATCOM to inject reactive current (d-axis current) into the AC grid. It should be emphasized that using the proposed method, since the AC grid current regulation, DC bus current regulation, and cell capacitor energy control is decoupled completely and $v_{o,com}^{*}$ is nullified, the DC bus current is nearly pure DC without fluctuation except switching frequency ripples. In Fig. 19, the experiment waveform of the DC bus current coincides with the theoretical waveform calculated as (46) by the model in Fig.6 (b) after the circuit breaker is switched on and validity of the modified modeling in Section III has been verified.

$$i_{dc,theo}=\frac{-V_{dc}^{*}}{R_{load}}\left\{1-\exp\left(-(t-t_{loaded})/\{(\frac{2}{3}L_o+L_{load})/R_{load}\}\right)\right\}. \quad (46)$$

VI. Conclusion

A new modified model of MMC for energy control of cell capacitor has been presented, which divides the MMC into AC grid current model, DC bus current model, and circulating current model. According to this modified model, the AC power control and the DC bus voltage control can be decoupled. And it is analytically described that the conventional cell capacitor energy control strategy with weak DC bus may cause some problems such as accumulated common mode component of leg internal voltages, the

TABLE I. Prototype Parameters

Quantity	Values
Number of cells per arm	6
Rated DC bus voltage (V_{dc}^{*})	210V
Rated cell capacitor voltage (V_{cell}^{*})	35V
Cell capacitor (C_{cell})	4.4mF
Grid line-to-line voltage (RMS)	80V
Arm inductor inductance (L_o)	2.0 mH
Arm inductor resistance (R_o)	5.0 mΩ
DC bus R-L load inductance (L_{load})	3.0 mH
DC bus R-L load resistance (R_{load})	53.6 Ω
Sampling frequency (f_{samp})	5.0 kHz
Switching frequency (f_{sw})	2.5 kHz

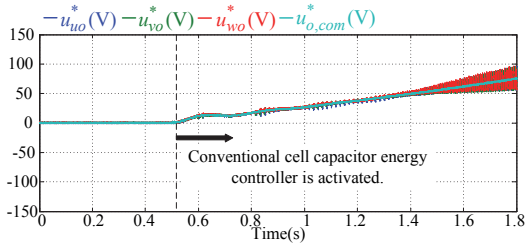

Figure 11. Leg internal voltages with the conventional method.

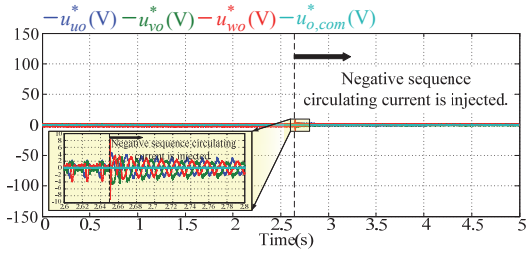

Figure 12. Leg internal voltages with the proposed method.

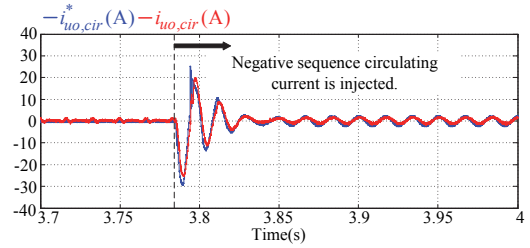

Figure 13. Phase *u* circulating current reference and circulating current when negative sequence circulating current is injected.

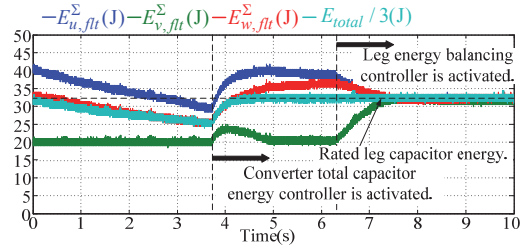

Figure 14. Leg capacitor energy before R-L load is connected.

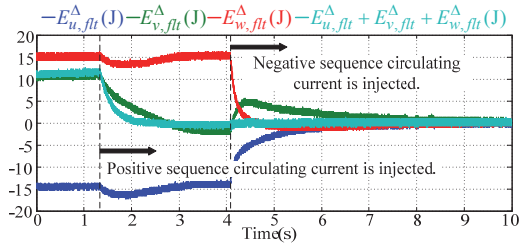

Figure 15. Upper and lower arm capacitor energy differences before R-L load is connected to the DC bus.

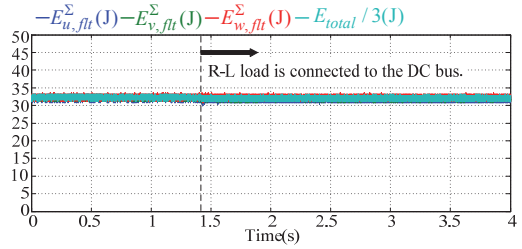

Figure 16. Leg capacitor energy after R-L load is connected.

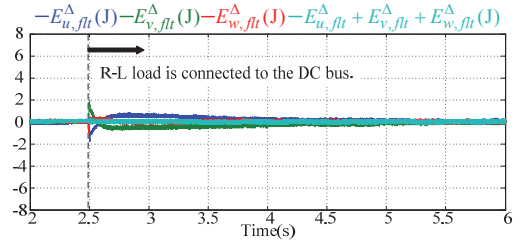

Figure 17. Upper and lower arm capacitor energy differences after R-L load is connected to the DC bus.

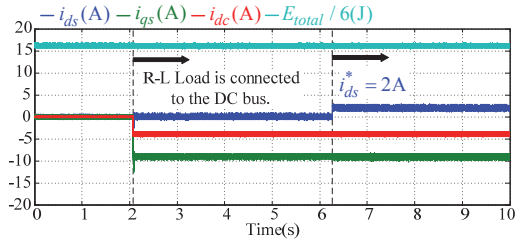

Figure 18. Grid current, DC bus current, and converter total energy after R-L load is connected to the DC bus.

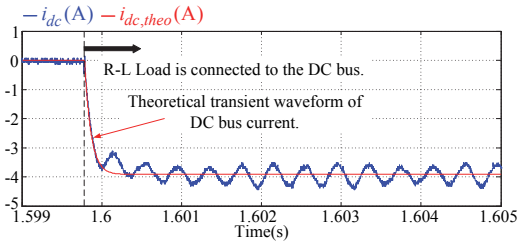

Figure 19. Experimental and theoretical DC bus current after R-L load is connected to the DC bus.

circulating current distortion, and instability of system. A new comprehensive cell capacitor energy control strategy has been proposed to solve these problems. With the proposed strategy, the leg capacitor energy has been well balanced by updating leg energy reference on-line and regulating DC component of circulating current. Upper and lower arm capacitor energy differences in three phases are eliminated uniformly by injecting both positive and negative sequence components in circulating current. The proposed strategy can prevent the common mode component of leg internal voltages inherently and improve capacitor energy control performance in view point of both dynamics and stability. The proposed control strategy completely decouples the AC grid current regulation, the DC bus current regulation, and the cell capacitor energy control and provides a solid base for control of MMCs in point-to-point or multi-terminal HVDC applications. The proposed control strategy has been also verified through experimental test.

REFERENCES

[1] T. K. Vrana and O. Fosso, "Technical aspects of the North Sea super grid," *CIGRE ELECTRA*, no. 258, pp. 6-19, Oct. 2011.

[2] S. Allebrod, R. Hamerski, and R. Marquardt, "New transformerless, scalable modular multilevel converters for HVDC-transmission," in *Proc. IEEE PESC*, 2008, pp. 174-179.

[3] B. Gemmell, J. Dorn, D. Retzmann, and D. Soerangr, "Prospects of multilevel VSC technologies for power transmission," in *Conf. Rec. IEEE-TDCE*, 2008, pp. 1-16. K. Elissa, "Title of paper if known," unpublished.

[4] A. Lesnicar and R. Marquardt, "An innovative modular multilevel converter topology suitable for a wide power range," in *Proc. IEEE Boogna Power Tech*, 2008, vol. 3, pp. 1-6.

[5] D. Peftitsis, G. Tolstoy, A. Antonopoulos, J. Rabkowski, J. K. Lim, M. Bakowski, L. Angquist, and H. P. Nee, "High-power modular multilevel converters with SiC JFETs," in *Proc. IEEE ECCE*, 2010, pp. 2148-2155.

[6] Rainer Marquardt, "Modular Multilevel Converter Topologies with DC-Short Circuit Current Llimitation," in *Proc. IEEE ECCE Asia*, 2011, pp. 1425-1431.

[7] AmirnaserYazdani, and Reza Iravani, "Voltage-Sourced Converters in Power Systems –Modeling, Control, and Applications," *IEEE Press*, 2011.

[8] Makoto Hagiwara, and Hirofumi Akagi, "Control and experiment of pulsewidth-modulated modular multilevel converters," in *IEEE Trans. Power Electronics.*, vol. 24, no. 7, pp. 1737-1746, Jul. 2009.

[9] Maryam Saeedifard, and Reza Iravani, "Dynamic performance of a modular multilevel back-to-back HVDC system," in *IEEE Trans. Power Delivery.*, vol. 25, no. 4, pp. 2903-2912, Oct. 2010.

[10] A Antonopoulos, L Anguist, and HP Nee, "On dynamics and voltage control of the modular multilevel converter," in *EPE European Conference on Power Electronics and Applications*, pp. 1-10, 2009.

[11] Jae-Jung Jung, Hak-Jun Lee, and Seung-Ki Sul, "Control strategy for improved dynamic performance of variable-speed drives with the Modular Multilevel Converter," in *IEEE Energy Conversion Congress and Exposition*, pp. 1481-1488, 2013.

[12] S. Rohner, S. Bernet, M. Hiller, and R. Sommer, "Modulation, losses, and semiconductor requirements of modular multilevel converters," in *IEEE Trans. Ind. Electron.*, vol. 57, no. 8, pp. 2633-2642, Aug. 2012.

[13] Q. R. Tu, Z. Xu, and L. Xu, "Reduced switching frequency modulation and circulating current suppression for modular multilevel converters," in *IEEE Trans. Power Del.*, vol. 26, no. 3 ,pp. 2009-2017, Jul. 2011.

[14] LennartAngquist, Antonios Antonopoulos, Daniel Siemaszko, KalleIlves, MichailVasiladiotis, and Hans-Peter Nee, "Open-loop control of modular multilevel converters using estimation of stored energy," in *IEEE Trans. Ind. Appli.*, vol. 47, no. 6, pp. 2516-2524, Nov. 2011.

[15] M. A. Perez, J. Rodriquez, "Generalized modeling and simulation of a modular multilevel converter," in *IEEE International Symposium on Industrial Electronics.*, pp. 1863-1868, 2011.